Desalination and Water Treatment
www.deswater.com
doi: 10.5004/dwt.2020.25923

196 (2020) 287–298
August

Removal of Orange G dye from water using halloysite nanoclay-supported ZnO nanoparticles

Ahlam A. Al-Beladi[a], Samia A. Kosa[a], Roswanira Abdul Wahab[b,c], Mohamed Abdel Salam[a,*]

[a]*Chemistry Department, Faculty of Science, King Abdulaziz University, P.O. Box: 80200, Jeddah 21589, Kingdom of Saudi Arabia, Tel. +966-541886660; Fax: +966-2-6952292; email: masalam16@hotmail.com (M.A. Salam), Tel. +966-507837549; Fax: +966-2-6952292; email: sweeet-moon@hotmail.com (A.A. Al-Beladi), Tel. +966-557627075; Fax: +966-2-6952292; email: skousah@kau.edu.sa (S.A. Kosa)*
[b]*Department of Chemistry, Faculty of Science, Universiti Teknologi Malaysia, 81310 Johor Bahru, Malaysia, Tel. +607-5510363; Fax: +607-5566162; email: roswanira@kimia.fs.utm.my (R.A. Wahab)*
[c]*Enzyme Technology and Green Synthesis Group, Universiti Teknologi Malaysia, 81310 Johor Bahru, Malaysia*

Received 26 August 2019; Accepted 6 April 2020

ABSTRACT

Zinc oxide nanoparticles (ZnO NPs) supported over halloysite nanoclay (ZnO/HS) were investigated for the removal of Orange G (OG) dye in simulated water and real water samples. This study aimed to synthesize ZnO NPs/HS to photo-catalytically degrade OG dye in the aforementioned water samples. In addition to establishing the kinetics and thermodynamics of the reaction. Surface and physicochemical characterizations affirmed the ZnO NPs/HS were mesoporous (61.0 m^2 g^{-1}) with the rod-shaped nanoparticles homogeneously dispersed over the surface of HS. Employment of ZnO/HS at a mass ratio of 3:47 (w/w) degraded the highest quantity of the dye, amounting to a mass loss of >100 mg in just 2 h (pH < 12). The UV-irradiated and direct sunlight-activated photodegradation of aqueous OG dye by ZnO/HS followed a first-order kinetic model with the latter exhibiting a higher rate constant (4.87×10^{-3} min^{-1}). Meanwhile, values of ΔG (−4.60 kJ mol^{-1}), ΔH (+42.8 kJ mol^{-1}), and ΔS (+159 J mol^{-1} K^{-1}) indicated that the ZnO/HS-UV-irradiated photodegradation process was entropically driven. The ZnO NPs/HS photocatalyst efficiently degraded OG dyes (49.78%–94.36%) dissolved in various real water samples, thus envisaging its applicability for convenient *in situ* photocatalytic treatment of contaminated water bodies.

Keywords: Photocatalytic; Kinetics; Nanoclay; Orange G dye; ZnO; Thermodynamics, Wastewater

1. Introduction

Azo dyes represent over 50% of all dyes in common use because of their chemical stability and versatility [1]. The high commercial dependence on azo dyes, however, highlights a major concern over their non-biodegradability, toxicity, and carcinogenicity. Dye-contaminated water bodies have been linked to a substantial increase in an array of complications in humans and aquatic animals, for instance, organ damage and respiratory disorders [2]. Hence, the elimination of such pollutants in water bodies is mandatory in ensuring a safe and clean environment. The toxicity of azo dyes is currently abated by using non-destructive processes, such as coagulation, activated carbon adsorption, and membrane filtration [3–5]. The treatment processes, however, are inadequate due to failure in achieving full degradation and mineralization of the dyes. While numerous methods are available to remove dyes in aquatic environments, the photocatalytic degradation approach is among the most convenient as it averts the use of any

* Corresponding author.

expensive chemicals. This method employs visible and solar light, thus necessitating rational designing and prudent selection of semiconductors showing optimum ratio and band edge positions, in order to harness the maximum potential of the developed photocatalyst [6–8].

At present, the *n*-type semiconductor zinc oxide (ZnO) has shown great potential as a catalyst to photo-catalytically degrade different types of water pollutants. This is due to its low cost, high activity, and environmentally friendly features which make it a promising contender for nanoparticle synthesis. The high surface area to volume ratio of ZnO nanoparticles (NPs) offers more surface-active sites to enable the preparation of highly effective photocatalytic systems [9,10]. As a popular strategy, highly effective ZnO photocatalytic systems have been designed and fabricated through chemical surface modifications by doping compounds with other metals or their oxides. Studies have documented that the technique considerably improves the photocatalytic ability of ZnO by (i) causing shifts in optical absorption, (ii) increasing surface defects, (iii) producing surface oxygen vacancies, and (iv) inhibiting the recombination of charge carriers [11–15]. Additionally, the photocatalytic removal of water pollutants by zinc oxide nanoparticles (ZnO NPs) can be accomplished by supporting the ZnO NPs on materials with inherently high surface area, *viz*. activated carbon [16], chitosan [17], graphene [18], carbon nanotubes [19], hexacyanoferrate nanocomposite [20], including three dimensional ordered macro-/mesoporous carbon [21].

Hence, the aforementioned fascinating ideas inspired this study to consider using a nanoclay-based nanomaterial as support for ZnO NPs. Moreover, this catalytic system has been demonstrated to be useful in improving the photocatalytic activities of several ZnOs [22–25]. In this research, the indigenously fabricated ZnO NPs were dispersed onto the surface of halloysite nanoclay to form a hybrid ZnO NPs/HS nanocomposite and used for the high-performance photocatalytic degradation of Orange G (OG) dye. It is worth mentioning here, the hybrid ZnO NPs/HS nanocomposite has yet to be investigated for the degradation of OG dye in simulated and real water samples, under solar and UV radiation. While the hybrid ZnO NPs/HS nanocomposite is a promising material for a broad range of applications, its feasibility alongside effectiveness to carry out the above reactions remains unknown.

In this study, the properties of ZnO NPs, HS, and ZnO NPs/HS nanocomposite were characterized using different chemical and physical techniques such as X-ray diffraction (XRD), scanning electron microscopy/energy-dispersive X-ray spectroscopy (SEM/EDX), transmission electron microscopy (TEM), ultraviolet-Vis diffuse reflectance spectra (UV-Vis-DRS) and surface area analyzer; while relevant operational photodegradation parameters (ratio of ZnO NPs/HS, mass, time, pH of solution and temperature) were optimized. Kinetics of the photoremediation reaction and the photocatalytic mechanism was also explored. The different thermodynamic parameters for the ZnO NPs/HS-solar assisted removal of OG dye, that is, Gibbs free energy, enthalpy, and entropy of the degradation were calculated, too. Finally, the efficacy of the ZnO NPs/HS photocatalyst was tested for the removal of OG dye dissolved in six different real water samples.

2. Materials and methods

2.1. Materials

Halloysite nanoclay; HS nanoclay, (685445 Aldrich), were obtained from Sigma-Aldrich Canada. All other chemicals used in this study were also obtained from Sigma-Aldrich (USA) (analytical grade), and all solutions were prepared using deionized water.

2.2. Preparation of ZnO NPs

ZnO NPs were synthesized by stirring a mixture of solutions of $ZnSO_4 \cdot 7H_2O$ (0.1 M) with NaOH (0.4 M) for 1 h at 80°C. The resultant ZnO NPs were precipitated, rinsed thrice in distilled water, and finally in acetone. The powder was dried overnight at room temperature and then calcined at 473 K for 60 min to obtain the ZnO NPs.

2.3. Preparation of ZnO NPs/HS nanocomposite

The ZnO NPs/HS nanocomposite was prepared by physically mixing ZnO NPs and HS nanoclay in a mortar till a homogeneous mixture was obtained.

2.4. Characterization techniques

XRD patterns were recorded for phase analysis and the measurement of crystallite size was performed on a Philips X-pert pro diffractometer, (United Kingdom). The instrument was operated at 40 mA and at 40 kV on CuKα radiation and a nickel filter in the 2θ range from 2° to 80° in steps of 0.02°, with a sampling time of one second per step. The estimation of the crystal size was done according to the Scherrer equation. Field emission scanning electron microscope (JSM-7500F, JEOL, Japan) equipped with an EDX accessory (Oxford EDS system), as well as a transmission electron microscope (TEM; type JEOL JEM-1230, Japan, operating at 120 kV, attached to a charged coupled device camera) and a scanning tunneling microscope (Agilent 5500, USA), were used to observe the morphology of each sample. A NOVA 3200e automated gas sorption system (Quantachrome, USA) was utilized to quantify the specific surface area of HS, ZnO NPs, and ZnO NPs/HS nanocomposite by Brunauer–Emmett–Teller (BET) method, taken at 77 K. ultraviolet-visible near infrared spectrophotometer (V-570 Jasco, Japan) was used to determine the UV-Vis-DRS and estimate the bandgap performance over the range 200−800 nm using the Tauc relation [26].

2.5. Photocatalytic degradation experiment

In a typical experiment, halloysite nanoclay (ZnO/HS) nanocomposite (100 mg) were dispersed in a 100 mL beaker containing various concentrations of OG solutions, and each mixture was magnetically stirred in darkness for 30 min to equilibrate adsorption–desorption of OG onto the photocatalyst surface. The experimental setup was located inside a box and assessed for the effects of natural solar light and UV light. An 8W Philip's lamp, (Netherlands) was utilized as the UV source and sited at a fixed distance of 25 cm from the top of the magnetic stir. An 8 mL aliquot of the mixture was withdrawn at designated time intervals, and the photocatalyst

was separated by filtration. The concentration of the remaining OG dye in each solution was read on an ultraviolet-visible spectrophotometer (UV-1650 PC, CPS-240A Shimadzu, USA) at 479 nm after the proper dilution with distilled water.

The removal efficiency of OG dye was estimated by applying the following equation:

$$\%\ \text{Photocatalytic degradation of OG dye} = \frac{100\times\left(C_0 - C_t\right)}{C_0} \quad (1)$$

where C_0 is the initial concentration of OG dye and C_t is the residual OG dye concentration in solution at a certain time (t).

The effect of different parameters on the photocatalytic degradation process was assessed for different calcination temperatures of ZnO NPs (373, 473, 573, 673, and 773 K) and calcination duration (30, 60, 90, 120, and 150 min). Other parameters assessed also included the ratio of mass ZnO/HS nanocomposite, contact time, mass, temperatures, and the pH of the solution.

It is noteworthy to mention that, all the experiments were repeated three times, and the reported values represent the averages. A control experiment was conducted in the absence of the photocatalyst to determine OG dye removed during the experiment due to the filtration, glassware, or any of the experimental equipment and found to be insignificant.

2.6. Real water samples collection

Tap water sample (TWS) was collected from a tap in our laboratory after allowing the water to flow for 10 min while the wastewater sample was collected from the membrane bio-reactor technology at a wastewater treatment plant ((MBR 6000 STP) at King Abdulaziz University Wastewater (KAUWW), Jeddah City (latitude deg. North 21.487954, longitude deg. East 39.236748). A sample of agricultural irrigation water was collected from the King Abdulaziz University (KAU), Jeddah City (latitude deg. North 21.484877, longitude deg. East 39.242104). Drinking water (Hana) and distilled water were sampled from a distillation unit in the laboratory, while the well water sample was collected from a deep well at Abdraboh AL-Beladi Farm; Khulais Province, Saudi Arabia (latitude deg. North 22.124376, longitude deg. East 39.500618). All real water samples were first filtered through a 0.45 μm Millipore filter paper, and stored in Teflon® bottles in darkness at 5°C.

3. Results and discussion

3.1. Characterization of ZnO NPs/HS

Fig. 1 illustrates the XRD patterns of ZnO NPs, halloysite nanoclay, and ZnO NPs/HS nanocomposite. The characteristic peaks of ZnO NPs were identified from three main diffraction peaks at 2θ = 31.72°, 34.38°, and 36.20° that corresponded to the (100), (002), and (101) crystal planes of hexagonal wurtzite ZnO (JCPDS file no.36–1451). The crystallite size of ZnO NPs as estimated from the Scherrer equation was 25.70 nm, while the observed HS nanoclay characteristic peaks were perfectly indexed to standard JCPDS file no.29–1487. The diffraction pattern of ZnO NPs/HS nanocomposite revealed the main characteristic peaks of hexagonal wurtzite ZnO, whereas most of the HS characteristic peaks were absent. This observation occurred previously with the combination of halloysite nanoclay with other metal oxides such as manganese dioxide [27], or metals such as Au–Ni nanoparticle [28]. This may be due to the high crystallinity of the ZnO NPs compared with the halloysite nanoclay.

Surface morphology and elemental chemical analysis of the ZnO NPs/HS nanocomposite were investigated by SEM equipped with EDX. As it is presented in Fig. 2, the SEM micrograph showed depositions of ZnO NPs on HS and, this was confirmed by EDX analysis that revealed the presence of Al, Si, O, and Zn as the main constituents of the ZnO NPs/HS nanocomposite. Correspondingly, the surface morphology of the ZnO NPs/HS nanocomposite was explored using TEM analysis. As is clear in Fig. 3, agglomerates of varying lengths of rod-shaped ZnO NPs with an average diameter of 25 nm were observed, agreeing well with the XRD measurement. The halloysite nanoclay appeared as hollow tubes of lengths and inner diameter between 1–15 microns and 10–150 nm respectively, alongside an average external- and internal diameter corresponding to 50 and 10 nm. Also, the TEM micrograph also showed the ZnO NPs were homogeneously distributed over the surface of the halloysite nanoclay.

The results for the nitrogen adsorption/desorption isotherms for ZnO NPs, HS, and ZnO NPs/HS nanocomposite are presented in Fig. 4. As can be seen, the N_2 adsorption/desorption isotherm for ZnO NPs, and HS was a type III isotherm, except the latter has an H4 type hysteresis loop while the former is a type III loop. This indicated the ZnO NPs and HS is a non-porous or macroporous solid and mesoporous, respectively, which corresponded well with the calculated BET specific surface of 17.9 and 72.8 $m^2\,g^{-1}$. This is because the smaller mesopores and higher surface area of HS permitted capillary condensation. It was verified that the combination of ZnO NPs with HS led to the formation of a mesoporous ZnO NPs/HS nanocomposite. This can be seen from the type III isotherm with an H4 type hysteresis loop, but the nanocomposite retained a relatively high BET specific surface area at 61.0 m^2g^{-1}. The appreciably expanded surface area of ZnO NPs/HS over the pure ZnO NPs indicated an increase in the available surface area of the nanocomposite for photocatalytic reactions. The high surface area of ZnO NPs/HS nanocomposite allows the adsorption of more OG dye, which could be reduced by the HS nanoclay which could be working as electron storage and facilitator [29].

The light absorption region and band gap are important factors to consider when developing any sort of photocatalyst and can be measured by UV-Vis-DRS. The absorption region and bandgap for ZnO NPs, HS, and ZnO NPs/HS nanocomposite were investigated, and the results are presented in Fig. 5. In general, the ZnO NPs were absorbed in the UV region with absorption edges corresponding to 400 and 423 nm. There was a notable decrease in band gap energies amounting between 3.1 and 2.93 eV, for the ZnO NPs, and ZnO NPs/HS nanocomposite, respectively, which indicated large reductions in energy band gaps upon mixing ZnO NPs with the HS nanoclay. With reductions in band gaps, the

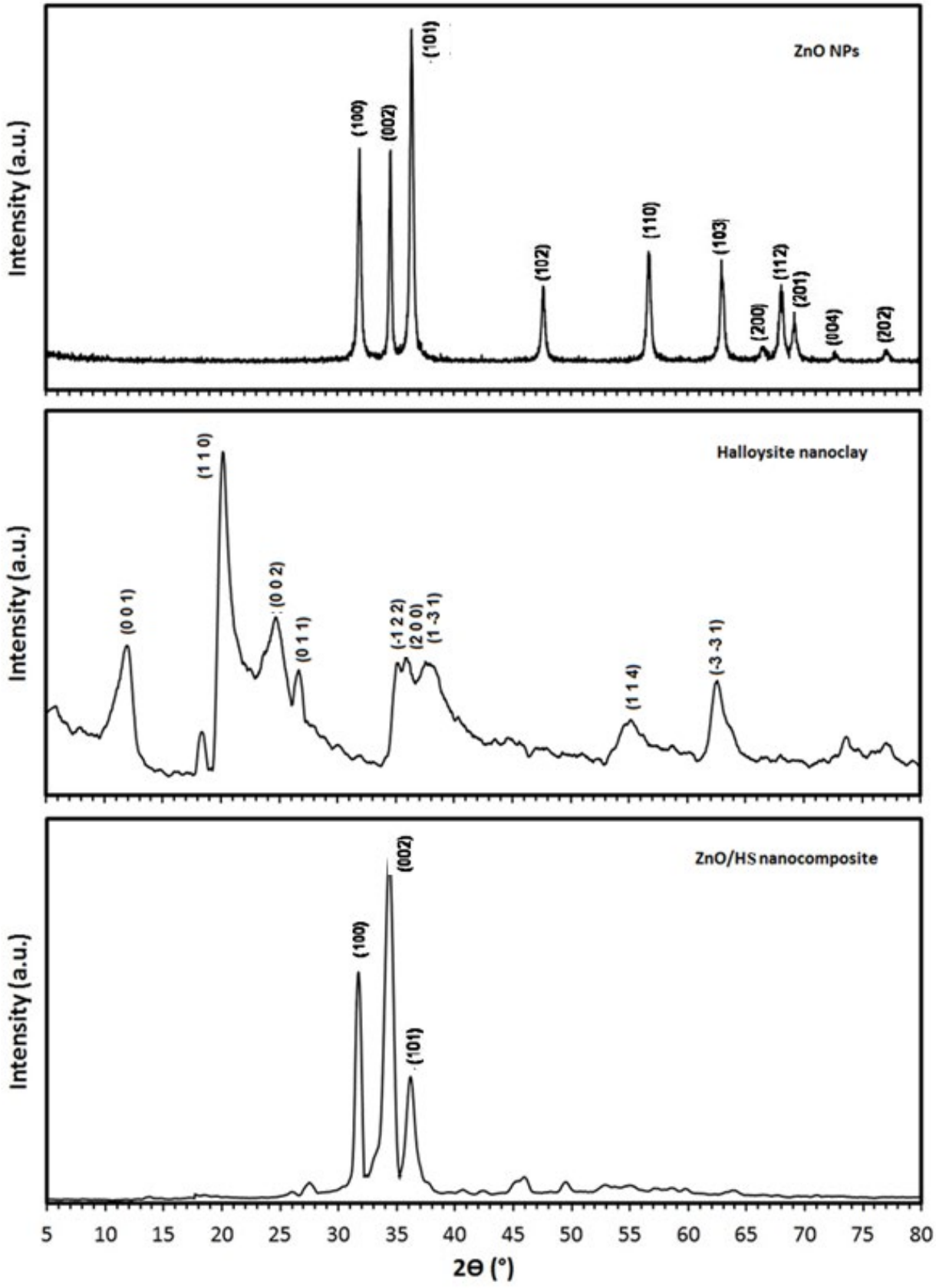

Fig. 1. XRD patterns of ZnO NPs, halloysite nanoclay, and ZnO NPs/HS nanocomposite.

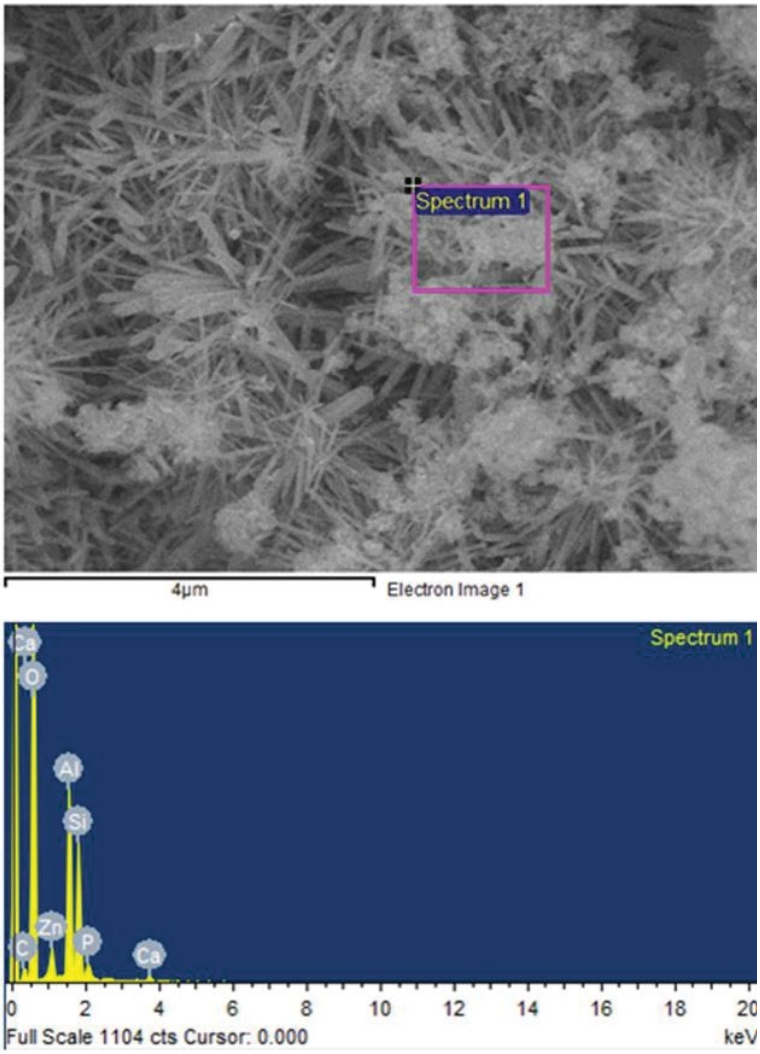

Fig. 2. SEM/EDX images of ZnO NPs/HS nanocomposite.

electron-hole recombination is anticipated, and the absorption shifts to the visible region. It appears that the dispersion of ZnO NPs over HS can modulate the environment of the ZnO lattice and influence the electronic band structure and create oxygen vacancies to reduce electron-hole pair recombination [30].

3.2. Photocatalytic degradation study

3.2.1. Optimization of the removal parameters

The effects of different parameters that affected the photocatalytic degradation of aqueous OG dye on ZnO NPs/HS nanocomposite were investigated and optimized. To monitor the effect mass ratios of ZnO NPs to HS on the ZnO/HS-catalyzed photocatalytic degradation of aqueous OG dye, a set of parallel experiments were performed using five different mass ratios; sample 1 (1:49), sample 2 (3:47), sample 3 (5:45), sample 4 (7:43), and sample 5 (10:40), of ZnO NPs to halloysite nanoclay. Fig. 6a indicated that all the nanocomposites (samples 2 to 5) showed higher photocatalytic degradation than the pure ZnO. samples 2 to 5 photo-catalytically degraded 72.6%, 80.0%, 76.6%, and 82.0% of OG dye, respectively, with removal capacities that corresponded to 570, 242, 160, 109.4, and 82 mg OG dye g^{-1} ZnO NPs. It was established that a mass ratio of ZnO NPs: HS nanoclay of 3:47 in sample 2 was the optimum, and gave the highest removal of aqueous OG dye per amount of ZnO NPs. The reason for the highest photocatalytic activity of the sample 2 ratio may have been due to the mechanical effect; as this ratio may be more stable mechanically compared with the other ratios. Also, it may have been due to the quantum size effect as this ratio of the ZnO NPs/HS nanocomposite increases the energy levels of the conduction band and valence band edges, which consequently enhances the redox potentials to employ the UV light in photocatalysis [31], and/or maybe due to the synergetic effect between ZnO NPs and HS nanoclay on the photocatalytic degradation of OG dye, and this synergetic effect reached its maximum with a weight ratio of 3:47. This synergetic effect, induced by a strong interphase interaction between ZnO NPs and HS nanoclay, was discussed in terms of different roles played by

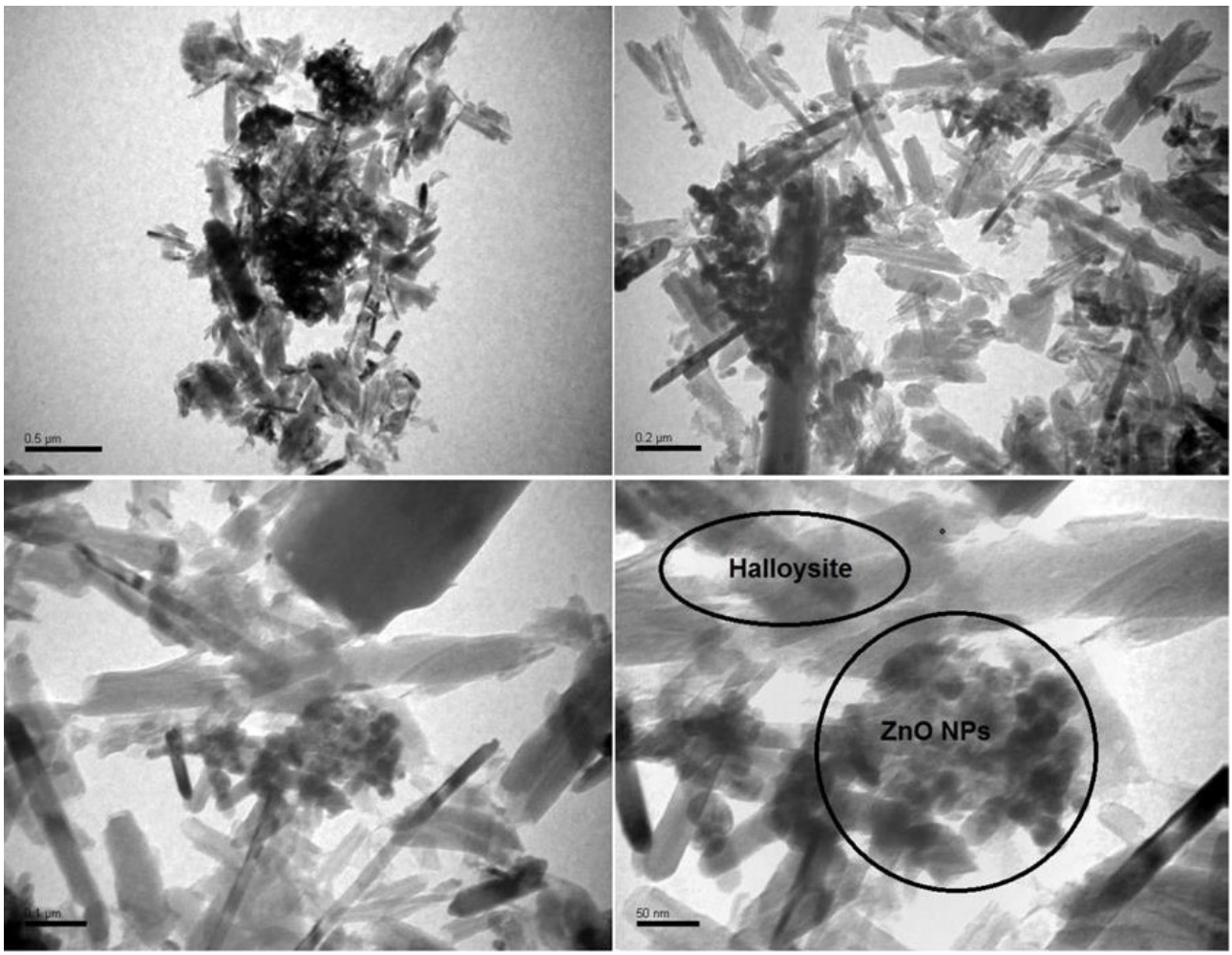

Fig. 3. TEM images of ZnO NPs/HS nanocomposite at different magnification power.

multi-walled carbon nanotubes in the composite catalysts. Moreover, the decrease in the photocatalytic activity with higher ZnO NPs/HS nanoclay mass ratio is considered to be related to the enhancement in the absorbing and scattering of photons in the photocatalytic reaction system [32]. Thus, the ratio was used for the subsequent dye removal experiments.

The effect of the ZnO NPs/HS nanocomposite mass on the photocatalytic degradation of aqueous OG dye was studied using dye concentrations of 50 mg L^{-1}, and the results are illustrated in Fig. 6b. As can be observed, the removal efficiencies of the dye increased from 0% to 24.1% when the amount the ZnO NPs/HS nanocomposite was increased from 10 to 120 mg. However, the degradation of aqueous OG dye dramatically increased from 23.57% to 90.92% following UV irradiation, likely attributed to the dose increase in the ZnO NPs/HS nanocomposite that provided a greater surface area and degradation sites for molecules of OG dye.

The removal time is one of the important factors that can greatly affect the efficiency of a removal process. Hence, the effect of contact time on the photocatalytic degradation of the OG dye by the ZnO NPs/HS nanocomposite was studied. Results revealed that increasing the contact time substantially improved the degradation process. Approximately 50.9% of aqueous OG dye was removed when equilibrium was reached after 360 min (Fig. 7a).

Another relevant factor to consider is the pH of the dye solution. The effect of solution pH on the degradation of aqueous OG dye over the ZnO NPs/HS nanocomposite was further for dye solutions with pH ranging from 3.0 to 12.0. Fig. 7b indicates the removal of OG dye by ZnO NPs/HS was highly dependent on the pH of the solution, following the sharp increase in dye removal from 22.61% to 76.29% with the increase of pH from 2.0 to 11.8. A possible reason for this has to do with the pKa value of the OG dye of 11.5 [33]. Thus, it is apparent that the OG dye is efficaciously removed by the ZnO NPs/HS nanocomposite, as long as the pH of the solutions is set to marginally below pH 12.

The temperature of the dye solution is another major factor that can affect a degradation process by a photocatalyst. This is because the removal efficiency of a certain pollutant from an aqueous solution is temperature-dependent, and hence it might affect the suitability of the catalyst. The effect of solution temperature on the degradation of OG dye by ZnO NPs/HS nanocomposite was studied at different temperatures; 298, 305, 321, and 328 K, and the results are presented in Fig. 7c. It was clear that raising the solution

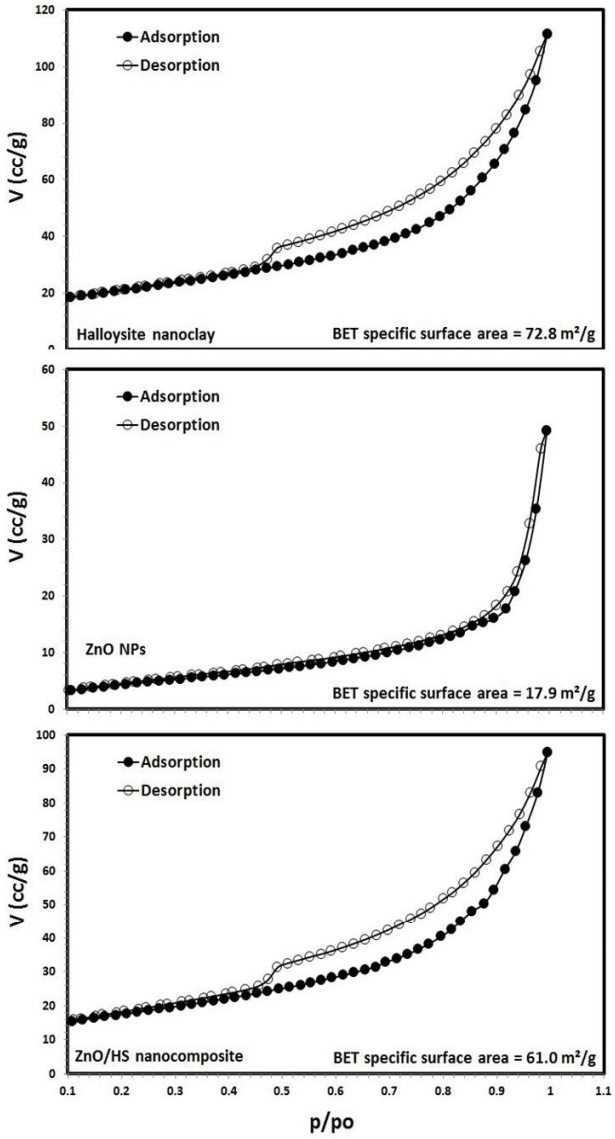

Fig. 4. BET surface area of halloysite nanoclay, ZnO NPs, and ZnO NPs/HS nanocomposite.

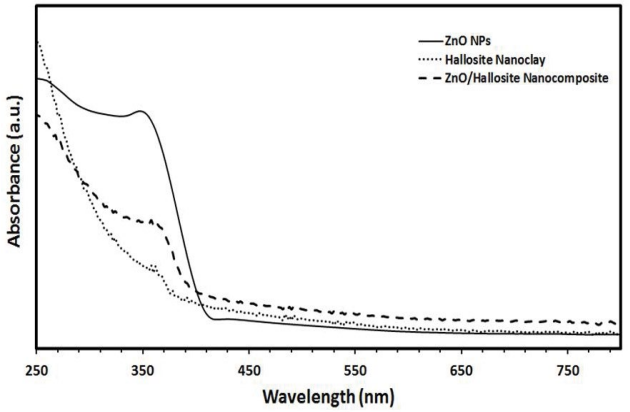

Fig. 5. UV-Vis-DRS of the ZnO NPs, halloysite nanoclay, and ZnO NPs/HS nanocomposite.

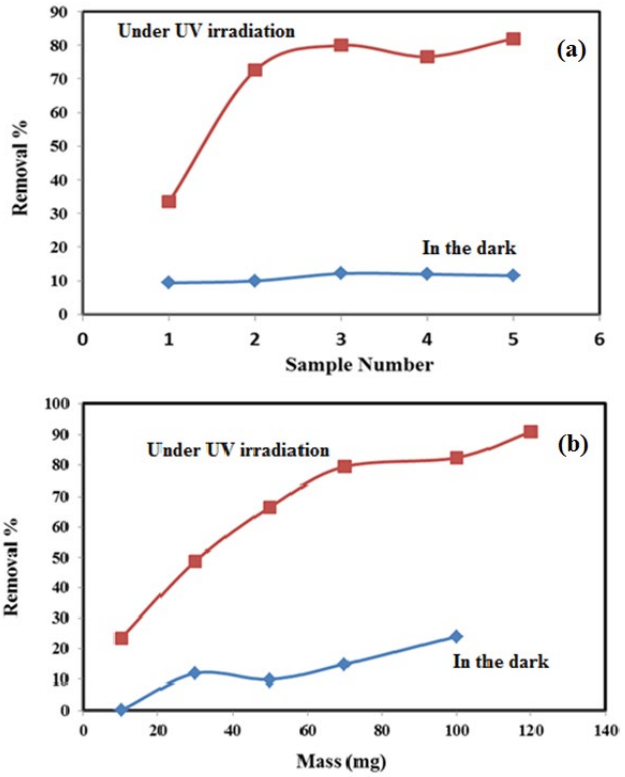

Fig. 6. (a) Effect of ZnO NPs/HS nanocomposite mass ratios and (b) effect of ZnO NPs/HS nanocomposite mass on the degradation of OG dye (experimental conditions: pH 8.5; 120.0 min contact time; sample volume 20 mL; OG dye concentration 50 mg L^{-1}).

temperature had a profound effect on aqueous OG dye removal by the ZnO NPs/HS nanocomposite. Increasing the temperature from 298 to 328 K led to the gradual increase in aqueous OG dye degradation from 47.07% to 81.12%. These results suggest that the removal process is endothermic in nature, which will be discussed further in the thermodynamic section.

It is well known that the main source of energy is the sun. Therefore, the photocatalytic degradation of the OG dye by ZnO NPs/HS nanocomposite was explored under direct sunlight. Fig. 8 shows the effect of contact time on the degradation of aqueous OG dye over ZnO NPs/HS nanocomposite under direct sunlight. It is was noted that the percentage degradation of the aqueous OG dye increased remarkably at the beginning of the experiment, and then reached equilibrium at 90.72% after 420 min (black points). The sunlight intensity (lux) increased with time till it reached a maximum value of 86.8 × 10^3 lux (after 240 min), beyond which it drastically reduced to hit the lowest point at 14.0 × 10^3 lux (after 480 min). It is noteworthy to mention that minor fluctuations in the temperature of aqueous OG dye occurred during the experimental period; 31°C to 36°C. This indicated that the removal of the aqueous OG dye was solely due to the photocatalytic degradation by the ZnO NPs/HS nanocomposite. Also, in comparison,

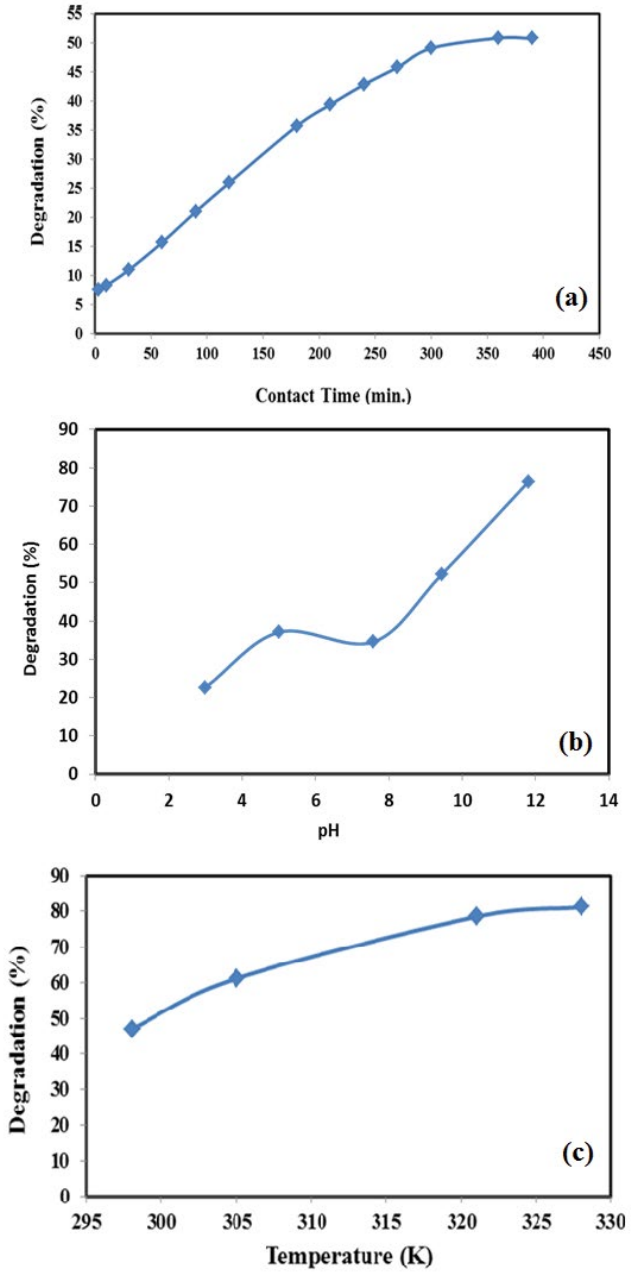

Fig. 7. (a) Effects of contact time, (b) solution pH, and (c) solution temperature, on the photodegradation of OG dye from aqueous solutions using ZnO NPs/HS nanocomposite (experimental conditions: 700 mg ZnO NPs/HS nanocomposite; volume 200 mL; OG dye concentration 50 mg L^{-1}).

the photodegradation of the OG dye under sunlight was greater than under UV irradiation. This may be because sunlight contains different light wavelengths, which may synergistically assist in the photodegradation process of the OG dye.

3.2.2. Kinetic and thermodynamic studies

Kinetic and thermodynamic studies for photocatalytic degradation of pollutants are vital in understanding

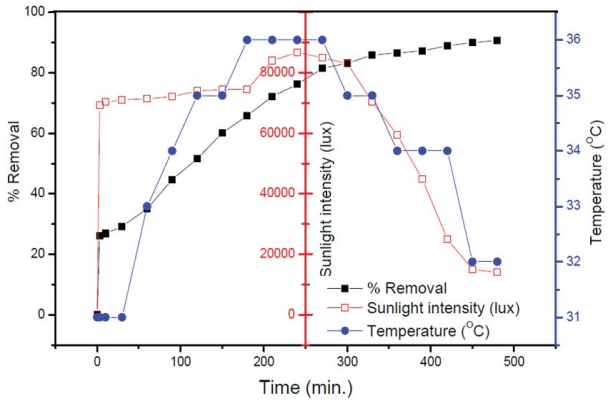

Fig. 8. The effects of contact time under sunlight on the removal of OG dye from aqueous solution by ZnO NPs/HS (experimental conditions: solution pH 8.5; 700 mg ZnO NPs/HS; sample volume 200 mL; OG dye concentration 50 mg L^{-1}).

the removal process in order to monitor and control the process. Fig. 9a illustrates the photocatalytic degradation efficiency of OG dye using ZnO NPs/HS nanocomposite under UV light. A gradual decrease in the concentration of aqueous OG dye over time till equilibrium was reached (after 240 min), was observed. To better understand this, the experimental data was treated kinetically using the most common and well-known kinetic model; a first-order kinetic model which is represented in a simplified form as:

$$\frac{dC}{dt} = -kC \tag{2}$$

$$\ln\frac{C_0}{C_t} = kt \tag{3}$$

where k is the rate constant of the photodegradation process, C_0 is the initial concentration of the OG dye and C_t is the concentration of OG dye after exposure to the light at time t (min.). The photodegradation curve of aqueous OG dye by the ZnO NPs/HS nanocomposite photocatalyst was well fitted by a mono-exponential curve, suggesting that the photodegradation experiment under UV irradiation followed the first-order kinetic model (Fig. 9c). Meanwhile, Fig. 9b revealed the photocatalytic degradation efficiency of aqueous OG dye using ZnO NPs/HS nanocomposite under direct sunlight. Clearly, a large portion of the dye was removed from the solution within 300 min of treatment. The photodegradation curve of aqueous OG dye by ZnO/HS under direct sunlight was also well fitted by a mono-exponential curve, suggesting that the UV irradiation photodegradation experiment also adhered to the first-order kinetic model (Fig. 9d). The calculated rate constants (k) were 2.09 × 10^{-3} min^{-1}, and 4.87 × 10^{-3} min^{-1} for the photocatalytic degradation of OG dye by the ZnO NPs/HS under UV irradiation and direct sunlight, respectively. From the k values, it was clear that irradiation of aqueous OG dye under direct sunlight showed a higher rate constant when

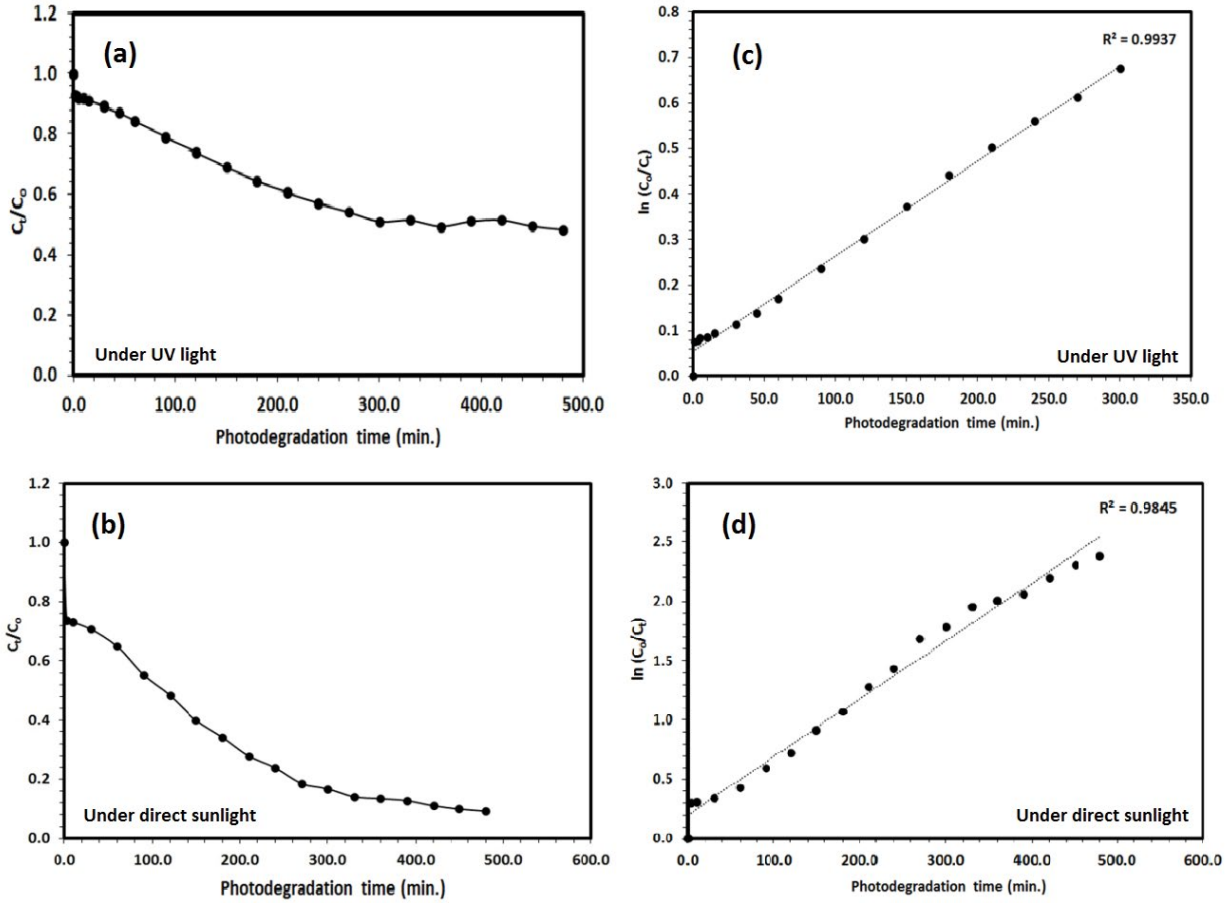

Fig. 9. The photocatalytic degradation efficiency of OG dye using ZnO NPs/HS nanocomposite under UV light (a), under direct sunlight (b), and the application of the first-order kinetic model (c) and (d). (Experimental conditions: solution pH 8.5; 700 mg ZnO NPs/HS nanocomposite; sample volume 200 mL; OG dye concentration 50 mg/L).

compared to UV irradiation, implying the suitability of ZnO NPs/HS for *in situ* degradation application of similar dyes.

Thermodynamic parameters; enthalpy change (ΔH), entropy change (ΔS), and Gibbs free energy change (ΔG), were calculated for the photocatalytic degradation of aqueous OG dye over the ZnO/HS photocatalyst under UV irradiation under different temperatures. Thermodynamic parameters were calculated using the variation of the thermodynamic distribution coefficient D with a change in temperature according to the equation [34,35]:

$$D = \frac{q_e}{C_e} \tag{4}$$

where q_e is the amount of OG dye molecules adsorbed and photo-catalytically degraded by ZnO NPs/HS nanocomposite photocatalyst (mg g^{-1}) at equilibrium, and C_e is the equilibrium concentration of OG dye in solution (mg L^{-1}). The ΔH and ΔS could be calculated according to the following equation:

$$\ln D = \frac{\Delta S}{R} - \frac{\Delta H}{RT} \tag{5}$$

A straight line was obtained by plotting ln$D$ vs. 1/T; as it is shown in Fig. 10, and the ΔH and ΔS values were calculated from the slope and the intercept of the straight line, respectively. The ΔG value was calculated at 298 K from the relation:

$$\Delta G = \Delta H - T\Delta S \tag{6}$$

The calculated ΔH, ΔS, and ΔG values were +42.8 kJ mol^{-1}, +159 J mol^{-1} K^{-1}, and −4.60 kJ mol^{-1}, respectively. The positive value of the enthalpy change indicated the endothermic nature of the photocatalytic degradation of aqueous OG dye by the ZnO NPs/HS nanocomposite. A positive value of the entropy change indicated the increase in the degree of freedom at the solid–liquid interface, while the negative value of the free energy change was as expected for a product favored and spontaneous process. Accordingly, the negative value of ΔG, and positive values of ΔH, and ΔS suggested that the photocatalysis of aqueous OG dye by nanoparticles of ZnO NPs/HS is entropically driven.

In general, it concluded that the removal of the OG dye from aqueous solution by ZnO NPs/HS nanocomposite followed both the adsorption and the photocatalytic degradation pathways, as the high surface area of ZnO NPs/

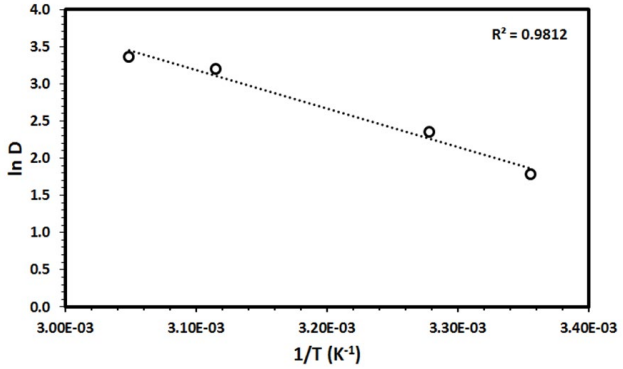

Fig. 10. The plot of ln*D* vs. 1/*T* for the thermodynamic parameter calculations for the photocatalytic degradation of OG dye in aqueous solution by ZnO NPs/HS under UV light. (Experimental conditions: 120.0 min contact time; solution pH 8.5; 50 mg ZnO NPs/HS; sample volume 20 mL; OG dye concentration 50 mg L^{-1}).

HS nanocomposite allows the adsorption of more OG dye, which is a consecutive step, could be degraded photocatalytically, as the HS nanoclay could be working as electron storage and facilitator.

3.2.3. Environmental applications

To study the applicability of ZnO NPs/HS nanocomposite for the removal of the OG dye, real environmental water samples must be investigated. Therefore, ZnO NPs/HS nanocomposite was added to six different water samples, collected from six different environmental sources. For brevity, the water sources were TWS, well water collected from a well Abdraboh AL-Beladi in Khulais province, Irrigation water sample collected from the KAU, drinking water (Hana), Distilled water collected from distillation device in the laboratory, and wastewater collected from KAUWW Treatment Plant. Principally, prior to the treatment, the measurement of the concentration of OG dye was performed through the real water samples, which showed the absence of the OG dye in the studied real samples. Accordingly, the samples were spiked with OG dye to obtain a final concentration of 50 ppm. The removal efficiency was calculated by comparing the concentrations of aqueous OG dye prior to and after the photocatalytic degradation under UV-irradiation. The results revealed that the developed ZnO NPs/HS nanocomposite successfully degraded 94.36%, 56.39%, 87.70%, 49.78%, 87.76%, and 81.30% of OG dye dissolved in tap water, wastewater, distilled water, well water, drinking water, and irrigation water, respectively (Fig. 11). The rather low photocatalytic degradation efficiencies of aqueous OG dye in both well water and wastewater may be due to the coexistence of other pollutants that competed for the same active sites on the ZnO NPs/HS nanocomposite. The satisfactory degradation of OG dye dissolved in the remaining water samples, thus indicating the suitability of the ZnO NPs/HS nanocomposite to photo-catalytically degrade organic dyes in polluted water bodies.

In general, the enhanced photocatalytic activity of ZnO NPs by supporting on HS nanoclay could be attributed to a

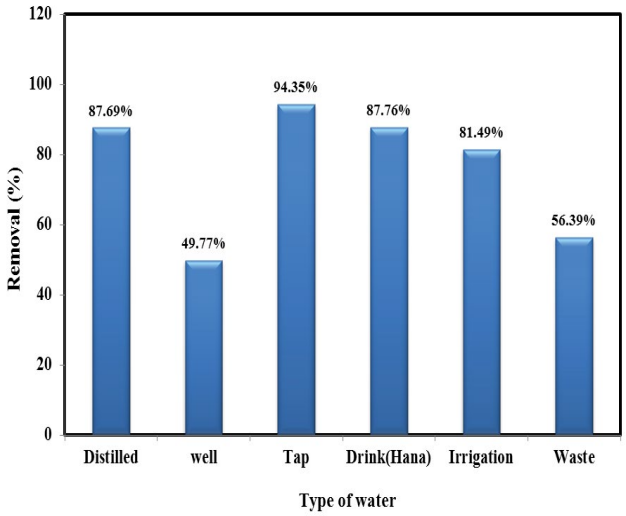

Fig. 11. Removal of OG dye from different environmental samples by ZnO NPs/HS under UV-irradiation (Experimental conditions: 20.0 ml; 120.0 min contact time; pH 8.5; 50.0 mg ZnO NPs/HS; OG dye concentrations 50.0 mg L^{-1}).

number of possible aspects, (i) the enhanced physicochemical properties of ZnO NPs, (ii) the highest concentration of active sites on ZnO NPs/HS nanocomposite, and (iii) the highest specific surface area of ZnO/HS nanocomposite compared to the unsupported ZnO NPs as the high surface area of ZnO NPs/HS nanocomposite allows the adsorption of more OG dye, which is a consecutive step, could be degraded photo-catalytically, as the HS nanoclay could be working as electron storage and facilitator. Furthermore, the study considered that the photocatalytic activity of ZnO/HS nanocomposite could be directly related to the decrease in the bandgap from 3.1 eV for the ZnO NPs to 2.93 eV for the ZnO/HS nanocomposite. This can be associated with the holes induced through the release of electrons (e^-) from valance band to conduction band under UV light illumination. Electrons in the conduction band can beneficially reduce the oxygen molecule to yield superoxide radicals, and holes generated in the conduction band may react with hydroxyl ions to form hydroxyl radicals. Moreover, studies have shown that these radicals are strong oxidative agents that lead to organic molecules converting into CO_2 and H_2O molecules [22,36,37]. Also, the UV irradiation could react and degraded the OG dye in three different pathways; the hydroxylation of the aromatic ring, desulfonation, and oxidative cleavage of the azo bond [38]. With reductions in the bandgap of ZnO NPs upon mixing with the HS, the electron-hole recombination is anticipated, and the absorption shifts to the visible region and facilitates the photo-degrading of the OG dye.

4. Conclusions

The study has shown that the ZnO NPs/HS was best prepared by calcining the ZnO NPs for 2 h at 200°C, to yield mesoporous and homogeneously dispersed rod-shaped ZnO NPs/HS over the surface of HS with a specific surface area of 61.0 m^2g^{-1}. Tests on the ZnO NPs/HS photocatalyst to

degrade aqueous OG dye in simulated water revealed that a mass ratio of ZnO:HS at 3:47 (w/w) degraded the highest quantity of the dye (>100 mg, 2 h, pH < 12). Although the photodegradation reactions catalyzed by UV-irradiation and direct sunlight-activation of ZnO/HS followed the first-order kinetic model, the latter was more efficacious (4.87×10^{-3} min^{-1}), while the UV-assisted degradation was found to be entropically driven. Most importantly, considering that the ZnO NPs/HS nanocomposite was successful in removing 49.78–94.36%, of OG dye in six samples of water (tap, wastewater, distilled water, well water, drinking water, irrigation water), it can be construed that the nanocomposite is a promising photocatalyst to assist in the convenient clean-up of water bodies contaminated with organic azo-based dyes.

References

[1] M. Neamtu, I. Siminiceanu, A. Yediler, A. Kettrup, Kinetics of decolorization and mineralization of reactive azo dyes in aqueous solution by the UV/H_2O_2 oxidation, Dyes Pigm., 53 (2002) 93–99.

[2] M. Stylidi, D.I. Kondarides, X.E. Verykios, Visible light-induced photocatalytic degradation of Acid Orange 7 in aqueous TiO_2 suspensions, Appl. Catal., B, 47 (2004) 189–201.

[3] G. Capar, U. Yetis, L. Yilmaz, Membrane based strategies for the pre-treatment of acid dye bath wastewaters, J. Hazard. Mater., 135 (2006) 423–430.

[4] A. Khaled, A. El Nemr, A. El-Sikaily, O. Abdelwahab, Removal of Direct N Blue-106 from artificial textile dye effluent using activated carbon from orange peel: adsorption isotherm and kinetic studies, J. Hazard. Mater., 165 (2009) 100–110.

[5] A. Szyguła, E. Guibal, M.A. Palacín, M. Ruiz, A.M. Sastre, Removal of an anionic dye (Acid Blue 92) by coagulation–flocculation using chitosan, J. Environ. Manage., 90 (2009) 2979–2986.

[6] G.G. Lenzi, C.V.B. Fávero, L.M.S. Colpini, H. Bernabe, M.L. Baesso, S. Specchia, O.A.A. Santos, Photocatalytic reduction of Hg(II) on TiO_2 and Ag/TiO_2 prepared by the sol–gel and impregnation methods, Desalination, 270 (2011) 241–247.

[7] H.Q. Wang, S.Y. Zhou, L. Xiao, Y.J. Wang, Y. Liu, Z.B. Wu, Titania nanotubes—a unique photocatalyst and adsorbent for elemental mercury removal, Catal. Today, 175 (2011) 202–208.

[8] X.L. Wang, S.O. Pehkonen, A.K. Ray, Photocatalytic reduction of Hg(II) on two commercial TiO_2 catalysts, Electrochim. Acta, 49 (2004) 1435–1444.

[9] N. Yusoff, L.-N. Ho, S.-A. Ong, Y.-S. Wong, W. Khalik, Photocatalytic activity of zinc oxide (ZnO) synthesized through different methods, Desal. Water Treat., 57 (2016) 12496–12507.

[10] C.C. Hu, L. Lu, Y.J. Zhu, R. Li, Y.J. Xing, Morphological controlled preparation and photocatalytic activity of zinc oxide, Mater. Chem. Phys., 217 (2018) 182–191.

[11] A. Phuruangrat, S. Siri, P. Wadbua, S. Thongtem, T. Thongtem, Microwave-assisted synthesis, photocatalysis and antibacterial activity of Ag nanoparticles supported on ZnO flowers, J. Phys. Chem. Solids, 126 (2019) 170–177.

[12] S. Rajaboopathi, S. Thambidurai, Synthesis of bio-surfactant based Ag/ZnO nanoparticles for better thermal, photocatalytic and antibacterial activity, Mater. Chem. Phys., 223 (2019) 512–522.

[13] A. Gaurav, R. Beura, J.S. Kumar, P. Thangadurai, Study on the effect of copper ion doping in zinc oxide nanomaterials for photocatalytic applications, Mater. Chem. Phys., 230 (2019) 162–171.

[14] P. Pascariu, I.V. Tudose, M. Suchea, E. Koudoumas, N. Fifere, A. Airinei, Preparation and characterization of Ni, Co doped ZnO nanoparticles for photocatalytic applications, Appl. Surf. Sci., 448 (2018) 481–488.

[15] A. Samanta, M.N. Goswami, P.K. Mahapatra, Optical properties and enhanced photocatalytic activity of Mg-doped ZnO nanoparticles, Physica E, 104 (2018) 254–260.

[16] H. Arfaeinia, H. Sharafi, M. Moradi, M. Ehsanifar, S.E. Hashemi, Efficient degradation of 4-chloro-2-nitrophenol using photocatalytic ozonation with nano-zinc oxide impregnated granular activated carbon (ZnO–GAC), Desal. Water Treat., 93 (2017) 145–151.

[17] K. Thirugnanasambandham, V. Sivakumar, Modeling and optimization of treatment of milk industry wastewater using chitosan–zinc oxide nanocomposite, Desal. Water Treat., 57 (2016) 18630–18638.

[18] B. Xue, Y.Q. Zou, High photocatalytic activity of ZnO–graphene composite, J. Colloid Interface Sci., 529 (2018) 306–313.

[19] D. Chaudhary, S. Singh, V.D. Vankar, N. Khare, ZnO nanoparticles decorated multi-walled carbon nanotubes for enhanced photocatalytic and photoelectrochemical water splitting, J. Photochem. Photobiol., A, 351 (2018) 154–161.

[20] Rachna, M. Rani, U. Shanker, Sunlight mediated improved photocatalytic degradation of carcinogenic benz[*a*]anthracene and benzo[*a*]pyrene by zinc oxide encapsulated hexacyanoferrate nanocomposite, J. Photochem. Photobiol., A, 381 (2019) 111861, https://doi.org/10.1016/j.jphotochem.2019.111861.

[21] F.X. Yin, Z. Zhang, Y.G. Zhang, C.W. Zhang, L.B. Xu, ZnO nanoparticles encapsulated in three dimensional ordered macro-/mesoporous carbon as high-performance anode for lithium-ion battery, Electrochim. Acta, 270 (2018) 274–283.

[22] H.B. Hadjltaief, S.B. Ameur, P. Da Costa, M.B. Zina, M.E. Galvez, Photocatalytic decolorization of cationic and anionic dyes over ZnO nanoparticle immobilized on natural Tunisian clay, Appl. Clay Sci., 152 (2018) 148–157.

[23] M. Akkari, P. Aranda, H. Ben Rhaiem, A. Ben Haj Amara, E. Ruiz-Hitzky, ZnO/clay nanoarchitectures: synthesis, characterization and evaluation as photocatalysts, Appl. Clay Sci., 131 (2016) 131–139.

[24] S.C. Motshekga, S.S. Ray, M.S. Onyango, M.N.B. Momba, Microwave-assisted synthesis, characterization and antibacterial activity of Ag/ZnO nanoparticles supported bentonite clay, J. Hazard. Mater., 262 (2013) 439–446.

[25] M. Akkari, P. Aranda, C. Belver, J. Bedia, A. Ben Haj Amara, E. Ruiz-Hitzky, ZnO/sepiolite heterostructured materials for solar photocatalytic degradation of pharmaceuticals in wastewater, Appl. Clay Sci., 156 (2018) 104–109.

[26] A. Kumar, Shalini, G. Sharma, Mu. Naushad, A. Kumar, S. Kalia, C.A. Guo, G.T. Mola, Facile hetero-assembly of superparamagnetic Fe_3O_4/$BiVO_4$ stacked on biochar for solar photo-degradation of methyl paraben and pesticide removal from soil, J. Photochem. Photobiol., A, 337 (2017) 118–131.

[27] W.B. Zhang, B. Mu, A.Q. Wang, Halloysite nanotubes template-induced fabrication of carbon/manganese dioxide hybrid nanotubes for supercapacitors, Ionic,s 21 (2015) 2329–2336.

[28] L. Jia, T. Zhou, J. Xu, X.H. Li, K. Dong, J.C. Huang, Z.Q. Xu, The enhanced catalytic activities of asymmetric Au–Ni nanoparticle decorated halloysite-based nanocomposite for the degradation of organic dyes, Nanoscale Res. Lett., 11 (2016), doi: 10.1186/s11671-016-1252-9.

[29] A. Kumar, G. Sharma, Mu. Naushad, T. Ahamad, R.C. Veses, F.J. Stadler, Highly visible active Ag_2CrO_4/Ag/$BiFeO_3$@RGO nano-junction for photoreduction of CO_2 and photocatalytic removal of ciprofloxacin and bromate ions: the triggering effect of Ag and RGO, Chem. Eng. J., 370 (2019) 148–165.

[30] P. Dhiman, Mu. Naushad, K.M. Batoo, A. Kumar, G. Sharma, A.S. Ghfar, G. Kumar, M. Singh, Nano $Fe_xZn_{1-x}O$ as a tuneable and efficient photocatalyst for solar powered degradation of bisphenol A from aqueous environment, J. Cleaner Prod., 165 (2017) 1542–1556.

[31] L.Q. Jiang, L. Gao, Fabrication and characterization of ZnO-coated multi-walled carbon nanotubes with enhanced photocatalytic activity, Mater. Chem. Phys., 91 (2005) 313–316.

[32] W.D. Wang, P. Serp, P. Kalck, J.L. Faria, Visible light photodegradation of phenol on MWNT-TiO_2 composite catalysts prepared by a modified sol–gel method, J. Mol. Catal. A: Chem., 235 (2005) 194–199.

[33] T. Wang, P. Zhao, N. Lu, H.C. Chen, C.L. Zhang, X. Hou, Facile fabrication of Fe_3O_4/MIL-101(Cr) for effective removal of acid

red 1 and orange G from aqueous solution, Chem. Eng. J., 295 (2016) 403–413.
[34] A. Bhatnagar, A.K. Minocha, B.-H. Jeon, J.-M. Park, Adsorptive removal of cobalt from aqueous solutions by utilizing industrial waste and its cement fixation, Sep. Sci. Technol., 42 (2007) 1255–1266.
[35] M. Abdel Salam, Coating carbon nanotubes with crystalline manganese dioxide nanoparticles and their application for lead ions removal from model and real water, Colloids Surf., A, 419 (2013) 69–79.
[36] Y. Zhou, F.S. Liu, S.T. Yu, Preparation and photo-catalytic activities of FeOOH/ZnO/MMT composite, Appl. Surf. Sci., 355 (2015) 861–867.
[37] A. Gnanaprakasam, V.M. Sivakumar, P.L. Sivayogavalli, M. Thirumarimurugan, Characterization of TiO_2 and ZnO nanoparticles and their applications in photocatalytic degradation of azodyes, Ecotoxicol. Environ. Saf., 121 (2015) 121–125.
[38] M.A. Meetani, M.A. Rauf, S. Hisaindee, A. Khaleel, A. AlZamly, A. Ahmad, Mechanistic studies of photoinduced degradation of Orange G using LC/MS, RSC Adv., 1 (2011) 490–497.